Plasmonic distributed feedback lasers at telecommunications wavelengths

Plasmonic distributed feedback lasers at telecommunications wavelengths

Milan J.H. Marell,[1] Barry Smalbrugge,[1] Erik Jan Geluk,[1] Peter J. van Veldhoven,[2] Beatrix Barcones,[2] Bert Koopmans,[2] Richard Nötzel,[2] Meint K. Smit,[1] and Martin T. Hill[1,*]

[1]*Dept. Electrical Engineering, Technische Universiteit Eindhoven, Postbus 513, 5600 MB, Eindhoven, The Netherlands*

[2]*Dept. Applied Physics, Technische Universiteit Eindhoven, Postbus 513, 5600 MB, Eindhoven, The Netherlands*

**m.t.hill@ieee.org*

Abstract: We investigate electrically pumped, distributed feedback (DFB) lasers, based on gap-plasmon mode metallic waveguides. The waveguides have nano-scale widths below the diffraction limit and incorporate vertical groove Bragg gratings. These metallic Bragg gratings provide a broad bandwidth stop band (~500nm) with grating coupling coefficients of over 5000/cm. A strong suppression of spontaneous emission occurs in these Bragg grating cavities, over the stop band frequencies. This strong suppression manifests itself in our experimental results as a near absence of spontaneous emission and significantly reduced lasing thresholds when compared to similar length Fabry-Pérot waveguide cavities. Furthermore, the reduced threshold pumping requirements permits us to show strong line narrowing and super linear light current curves for these plasmon mode devices even at room temperature.

OCIS codes: (250.5403) Plasmonics; (250.5960) Semiconductor lasers.

References and links

1. M. T. Hill, Y.-S. Oei, B. Smalbrugge, Y. Zhu, T. de Vries, P. J. van Veldhoven, F. W. M. van Otten, T. J. Eijkemans, J. P. Turkiewicz, H. de Waardt, E. J. Geluk, S.-H. Kwon, Y.-H. Lee, R. Nötzel, and M. K. Smit, "Lasing in metallic-coated nanocavities," Nat. Photonics **1**(10), 589–594 (2007).
2. M. A. Noginov, G. A. Zhu, A. M. Belgrave, R. Bakker, V. M. Shalaev, E. E. Narimanov, S. Stout, E. Herz, T. Suteewong, and U. Wiesner, "Demonstration of a spaser-based nanolaser," Nature **460**(7259), 1110–1112 (2009).
3. R. F. Oulton, V. J. Sorger, T. Zentgraf, R.-M. Ma, C. Gladden, L. Dai, G. Bartal, and X. Zhang, "Plasmon lasers at deep subwavelength scale," Nature **461**(7264), 629–632 (2009).
4. R. Perahia, T. P. M. Alegre, A. H. Safavi-Naeini, and O. Painter, "Surface-plasmon mode hybridization in subwavelength microdisk lasers," Appl. Phys. Lett. **95**(20), 201114 (2009).
5. K. Yu, A. Lakhani, and M. C. Wu, "Subwavelength metal-optic semiconductor nanopatch lasers," Opt. Express **18**(9), 8790–8799 (2010).
6. M. P. Nezhad, A. Simic, O. Bondarenko, B. Slutsky, A. Mizrahi, L. Feng, V. Lomakin, and Y. Fainman, "Room-temperature subwavelength metallo-dielectric lasers," Nat. Photonics **4**(6), 395–399 (2010).
7. S. H. Kwon, J. H. Kang, C. Seassal, S. K. Kim, P. Regreny, Y. H. Lee, C. M. Lieber, and H. G. Park, "Subwavelength plasmonic lasing from a semiconductor nanodisk with silver nanopan cavity," Nano Lett. **10**(9), 3679–3683 (2010).
8. D. J. Bergman and M. I. Stockman, "Surface plasmon amplification by stimulated emission of radiation: quantum generation of coherent surface plasmons in nanosystems," Phys. Rev. Lett. **90**(2), 027402 (2003).
9. S.-W. Chang, T.-R. Lin, and S. L. Chuang, "Theory of plasmonic Fabry-Perot nanolasers," Opt. Express **18**(14), 15039–15053 (2010).
10. J. Huang, S.-H. Kim, and A. Scherer, "Design of a surface-emitting, subwavelength metal-clad disk laser in the visible spectrum," Opt. Express **18**(19), 19581–19591 (2010).
11. R. Zia, M. D. Selker, P. B. Catrysse, and M. L. Brongersma, "Geometries and materials for subwavelength surface plasmon modes," J. Opt. Soc. Am. A **21**(12), 2442–2446 (2004).
12. M. T. Hill, M. Marell, E. S. P. Leong, B. Smalbrugge, Y. Zhu, M. Sun, P. J. van Veldhoven, E. J. Geluk, F. Karouta, Y.-S. Oei, R. Nötzel, C.-Z. Ning, and M. K. Smit, "Lasing in metal-insulator-metal sub-wavelength plasmonic waveguides," Opt. Express **17**(13), 11107–11112 (2009).
13. J. Buus, M. Amann, and D. Blumenthal, *Tunable Laser Diodes and Related Optical Sources* (John Wiley & Sons, 2005).

#146774 - $15.00 USD Received 28 Apr 2011; revised 12 Jun 2011; accepted 14 Jun 2011; published 21 Jul 2011

14. S. Nilsson, T. Kjellberg, T. Klinga, R. Schatz, J. Wallin, and K. Streubel, "Improved spectral characteristics of MQW-DFB lasers by incorporation of multiple phase-shifts," J. Lightwave Technol. **13**(3), 434–441 (1995).
15. W. Zhang, L. J. Wang, J. C. Zhang, Q. D. Zhang, L. Li, J. Q. Liu, F. Q. Liu, and Z. G. Wang, "Stable single-mode distributed feedback quantum cascade laser with surface metal grating," J. Phys. D Appl. Phys. **43**(38), 385103 (2010).
16. B. G. Lee, M. A. Belkin, R. Audet, J. MacArthur, L. Diehl, C. Pflügl, F. Capasso, D. C. Oakley, D. Chapman, A. Napoleone, D. Bour, S. Corzine, G. Höfler, and J. Faist, "Widely tunable single-mode quantum cascade laser source for mid-infrared spectroscopy," Appl. Phys. Lett. **91**(23), 231101 (2007).
17. Z. Han, E. Forsberg, and S. He, "Surface plasmon Bragg gratings formed in metal-insulator-metal waveguides," IEEE Photon. Technol. Lett. **19**(2), 91–93 (2007).
18. F. Kusunoki, T. Yotsuya, J. Takahara, and T. Kobayashi, "Propagation properties of guided waves in index-guided two-dimensional optical waveguide," Appl. Phys. Lett. **86**(21), 211101 (2005).
19. P. B. Johnson and R. W. Christy, "Optical constants of the noble metals," Phys. Rev. B **6**(12), 4370–4379 (1972).
20. M. T. Hill, "Metallic nano-cavity lasers at near infrared wavelengths," Proc. SPIE **7394**, 739409 (2009).
21. M. J. H. Marell, "Gap plasmon mode distributed feedback lasers," PhD Dissertation, Eindhoven University of Technology, The Netherlands, (2010).
22. J.-K. Hwang, H.-Y. Ryu, and Y.-H. Lee, "Spontaneous emission rate of an electric dipole in a general microcavity," Phys. Rev. B **60**(7), 4688–4695 (1999).
23. E. Yablonovitch, "Inhibited spontaneous emission in solid-state physics and electronics," Phys. Rev. Lett. **58**(20), 2059–2062 (1987).
24. P. Lodahl, A. Floris Van Driel, I. S. Nikolaev, A. Irman, K. Overgaag, D. Vanmaekelbergh, and W. L. Vos, "Controlling the dynamics of spontaneous emission from quantum dots by photonic crystals," Nature **430**(7000), 654–657 (2004).
25. R.-M. Ma, R. F. Oulton, V. J. Sorger, G. Bartal, and X. Zhang, "Room-temperature sub-diffraction-limited plasmon laser by total internal reflection," Nat. Mater. **10**(2), 110–113 (2011).
26. G. P. Agrawal and N. K. Dutta, *Semiconductor Lasers*, 2nd ed. (Van Nostrand Reinhold, 1993).
27. E. Yablonovitch, R. Bhat, C. E. Zah, T. J. Gmitter, and M. A. Koza, "Nearly ideal InP/$In_{0.53}Ga_{0.47}As$ heterojunction regrowth on chemically prepared $In_{0.53}Ga_{0.47}As$ surfaces," Appl. Phys. Lett. **60**(3), 371–373 (1992).
28. A. Forchel, A. Menschig, B. E. Maile, H. Leier, and R. Germann, "Transport and optical properties of semiconductor quantum wires," J. Vac. Sci. Technol. B **9**(2), 444–450 (1991).
29. E. Zielinski, H. Schweizer, K. Streubel, H. Eisele, and G. Weimann, "Excitonic transitions and exciton damping processes in InGaAs/InP," J. Appl. Phys. **59**(6), 2196–2204 (1986).

1. Introduction

Lasers based on metallic cavities have opened up a new route for laser miniaturization in the last few years [1–7]. The myriad of concepts presented include propagating plasmon mode devices, an example of the SPASER concept [8] which is deep-subwavelength in all three dimensions, and metal encapsulated devices which tightly confine the light to close to the diffraction limit or even below in some dimensions. Most devices are optically pumped and use dye or semiconductor gain medium, however some semiconductor devices are electrically pumped, which brings them closer to applications. Furthermore, there has also been work looking at the theory behind such devices [9,10], showing that some designs have the potential for useful devices.

One of the most promising approaches for both the construction of lasers, active and passive components with true sub-wavelength size is the use of metal-insulator-metal (MIM) waveguide structures which guide gap-plasmon modes [11]. Lasing in Fabry-PérotPérot (FP) cavities made from sections of such metallic waveguides has already been shown [12]. However, for many applications the precise control of the lasing wavelength and the optical mode in a waveguide laser cavity is highly desirable. Additionally, for optical signal processing applications and also out-coupling of laser light to passive waveguides, some form of mirror with controlled reflectivity and frequency selection is required. Incorporation of Bragg gratings into the waveguide to form distributed feedback (DFB) or distributed Bragg reflectors (DBR) [13,14] is common in dielectric devices and also plasmonic structures operating in the far-infrared [15,16].

To implement Bragg type reflectors in an MIM waveguide structure, the width of the MIM waveguide can be modulated to form vertical groove gratings [17] as shown in Fig. 1. Broad high reflectivity stop bands are possible in such structures (Fig. 2). The optical intensity plots (obtained from finite difference time domain FDTD simulations) for the resonant modes that occur in such waveguide grating structures are given in Fig. 3.

#146774 - $15.00 USD Received 28 Apr 2011; revised 12 Jun 2011; accepted 14 Jun 2011; published 21 Jul 2011

Our version of the MIM waveguide includes a thin insulator region between the semiconductor and metal (metal insulator semiconductor insulator metal - MISIM waveguide), and contains a higher index gain region (InGaAs) to localize the propagating mode [12,18]. Additionally the InGaAs gain region is pumped via an electrical n-contact located on the top of the ridge and p-contact via the substrate [12] (Fig. 1). We have chosen a simple InGaAs gain medium due to our experience in growing it. A quantum well gain medium may be a better alternative [6].

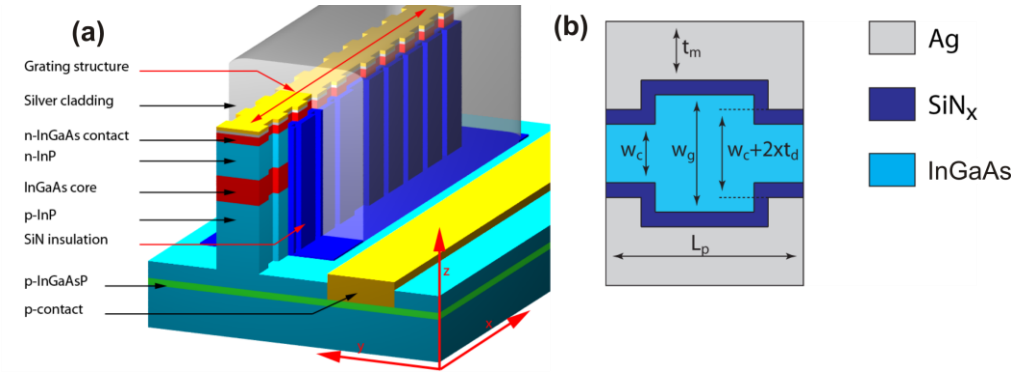

Fig. 1. (a) Schematic overview of the device. The semiconductor core consists of an InP/InGaAs/InP heterojunction. The core is shielded from the silver cladding by a SiN_x layer. (b) Shows a top view of a single grating section.The characteristic parameters of the structure are w_c, w_g and L_p, which represent the width of the waveguide core, the width of a grating section and the period of the grating. t_m and t_d are the thicknesses of the metal cladding and dielectric insulation layer respectively. A quarter wavelength phase shift is placed in the center of the grating.

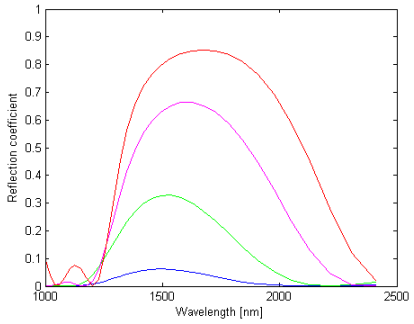

Fig. 2. Typical reflection spectrum from a three period vertical groove grating, based on the M-I-S-I-M waveguide structure, w_c = 100 nm + x nm, red x = 80, magenta x = 60, green x = 40, blue x = 20, t_d = 20 nm .

#146774 - $15.00 USD Received 28 Apr 2011; revised 12 Jun 2011; accepted 14 Jun 2011; published 21 Jul 2011

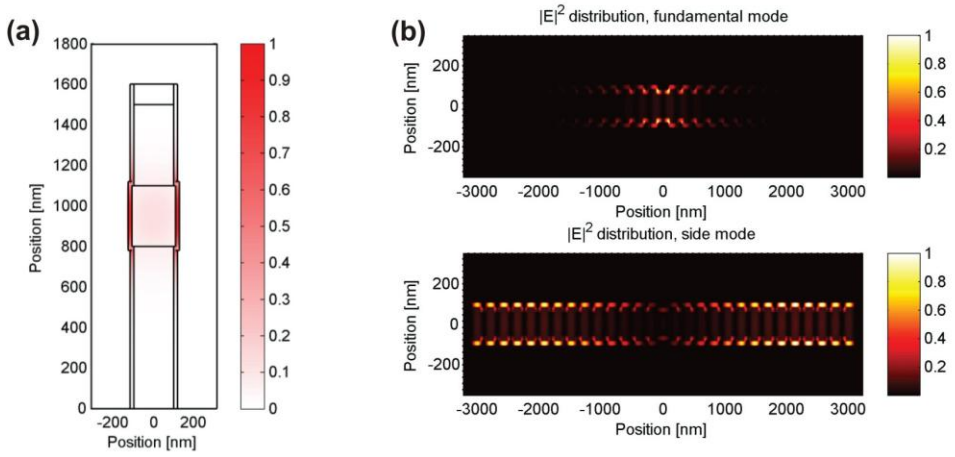

Fig. 3. (a) Simulated electric field intensity ($|E|^2$) plot of a slice through the waveguide (z = 0 plane). The plot shows the existence of a well confined cavity mode centred on the InGaAs layer. Furthermore, that the field is strongest in the SiN_x region between the semiconductor and the metal. (b) Field distribution of the mode at the Bragg wavelength with the mode centered on the quarter wavelength phase shift, and also at the first band-edge mode, where the mode is spread out through the grating. Plots show slices through the z = 0 plane.

2. Device fabrication

The InP/InGaAsP/InGaAs layer stack [1] as shown in Fig. 1 and Fig. 3a was grown via metal organic vapour phase epitaxy on a double polished semi-insulating InP substrate. All InGaAsP/InGaAs layers were lattice matched to InP. Electron beam lithography and reactive ion etching (RIE) was used to form a SiO_2 hard mask to define the ridge/DFB cross sections. The ridge was formed by inductively coupled plasma (ICP) RIE, then a number of surface oxidation and wet chemical oxide removal steps, to remove surface damage and modify the sidewall profile.

The silicon nitride layer was deposited using plasma enhanced chemical vapor deposition. Planarization with resist was used to expose just the tops of the pillars, to form the top n-contact. Various metal layers were deposited mostly via electron beam evaporation. However, the silver encapsulation was deposited via thermal evaporation and annealed at 400°C for 60 seconds. A lateral p-contact was formed via the p-InGaAsP layer.

The processed wafer was cleaved into sections containing eight devices. The sections were mounted with the substrate facing up on carriers, and wire bonds made to individual devices. For selected devices focused ion beam milling was used to open the end facets of the MIM waveguides, to allow direct measurement of light travelling along the waveguides. Figure 4 shows scanning electron microscope (SEM) pictures of a section of the semiconductor waveguide core before encapsulation in metal (silver), and a cross-section of one of the waveguides.

#146774 - $15.00 USD Received 28 Apr 2011; revised 12 Jun 2011; accepted 14 Jun 2011; published 21 Jul 2011

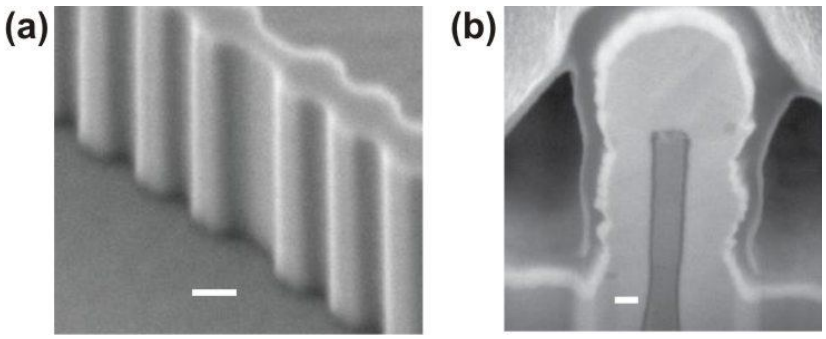

Fig. 4. (a) Scanning electron microscope (SEM) photo of the DFB structure without the surrounding silver and nitride layer. All scale bars represents 100 nm. (b) A cross-section of DFB structure, with surrounding silver and gold layers. The dark line between the metal cladding and the semiconductor core is the nitride insulation layer. The width of the semiconductor core is approximately 100 nm.

3. Waveguide modes

For the gap-plasmon (Transverse Magnetic, TM_0) modes that propagate in such waveguides, a significant proportion of the modal energy is carried in the thin insulator region between the metal and semiconductor (Fig. 3a). Small changes in the width of the waveguide core can result in a large modal mismatch and a strong reflection, which can be used to achieve Bragg grating coupling coefficients 10 to 100 times larger than in dielectric gratings. From FDTD simulations of a section of grating length L, the reflectivity R can be found, and from this the grating coupling coefficient $\kappa = \tanh^{-1}(R^{1/2})/L$ can be shown to reach 5000 cm^{-1} over a bandwidth of 500 nm, centered at 1550 nm. The M-I-S-I-M waveguide parameters for the above grating were (Fig. 1b): w_c = 100 nm, $w_g = w_c + 50$ nm, L_p = 230 nm, t_d = 20 nm. A cavity made from two such gratings with a quarter wavelength shift between them should have a quality factor (Q) of ~300 at room temperature. This Q is primarily determined by the optical losses in the metal [19]. The optical gain from the InGaAs required to overcome losses in the cavity can be found [20] to be approximately 1200 cm^{-1}, a value which can be obtained from bulk InGaAs material. (Fabry-Perot devices have a similar Q and modal confinement, and hence a similar threshold gain). The strong grating coupling means only a few periods (<20) are required to achieve a Q of 300, potentially resulting in devices with lengths less than 4 microns. Reducing the grating periods on one side of the quarter wavelength shift would allow for out coupling of some light into a waveguide. However, with the base threshold gain being ~1200 cm^{-1} at room temperature, there is likely only potential for extraction of a few tens percent of the light in the cavity [9,10].

Changing the period of the grating can tune the Bragg wavelength, for example, a change of 60 nm in period can tune the wavelength by 400 nm, in the region of 1550 nm.

4. Device measurement

A series of devices were made with the structure described above. The core waveguide width was varied from 80 nm to 180 nm. Furthermore the grating period was varied from 180 to 240 nm. The processed devices were placed in a variable-temperature liquid nitrogen cryostat which was cooled to 80K and 296K. The device was forward biased with a DC current source for the 80K measurements. For measurements at 296K a pulsed voltage source was used with 50 ns pulse width, 1 MHz repetition rate. The laser light escaping through the substrate was collected by a microscope objective. Half of the light went to a camera system to facilitate alignment. The other half was coupled into a single mode fiber which then fed the emitted light to either a spectrometer or a power meter. The spectrometer had a minimum resolution bandwidth limit of ~0.4 nm. A linear film polarizer was also placed in the light path after the microscope objective. The polarizer allowed us to determine if the largest electric field vector

#146774 - $15.00 USD Received 28 Apr 2011; revised 12 Jun 2011; accepted 14 Jun 2011; published 21 Jul 2011

of the light was TM (perpendicular to waveguide sidewall) or TE (parallel to waveguide sidewall) polarized. Light collected via the substrate for the TE mode has the strongest electric field vector parallel to the waveguide, inspite of the fact that the strongest electric field component inside the waveguide is in the vertical direction [21].

Optical spectra for one of the DFB devices measured at 80K are shown in Fig. 5 (this particular device had parameters w_c = 140 nm +/– 10 nm, w_g = 190 nm, L_p = 230 nm and t_d = 15 nm). The spectra show the emergence of a single narrow spectral line with increased pumping. The final measured line width was limited by the spectrometer resolution at ~0.4 nm. Below threshold linewidths indicated a cavity Q on the order of 300 or less. The ratio between the main peak and any side modes was over 21 dB, and the light emission was strongly TM polarized, consistent with a gap-plasmon mode propagating in the MIM waveguide [11]. The light current curve for the DFB device is given in Fig. 6a, and shows a threshold like behavior for the lasing mode, at around 500 μA.

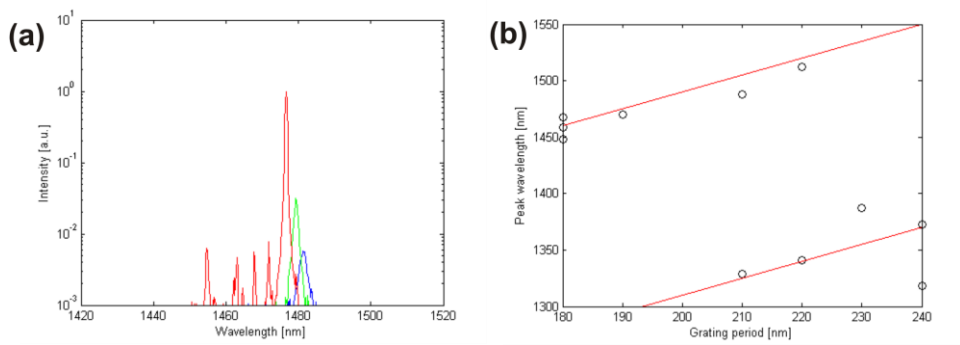

Fig. 5. (a) A number of spectra at various injection currents with core width w_c ~140nm at 80K, blue 500 μA, green 700 μA, red 3000 μA. Far above threshold the laser peak is 21 dB above any other grating peaks. Note the near absence of any spontaneous emission pedestal. The wavelength shift due to higher current is due to reduced refractive index at higher carrier densities. (b) Plot of lasing wavelength of a number of DFB lasers versus the grating period. Points clustered on the upper line represent devices which lased at the grating Bragg wavelength. Points clustered on the lower line represent devices which lased at a grating band edge wavelength.

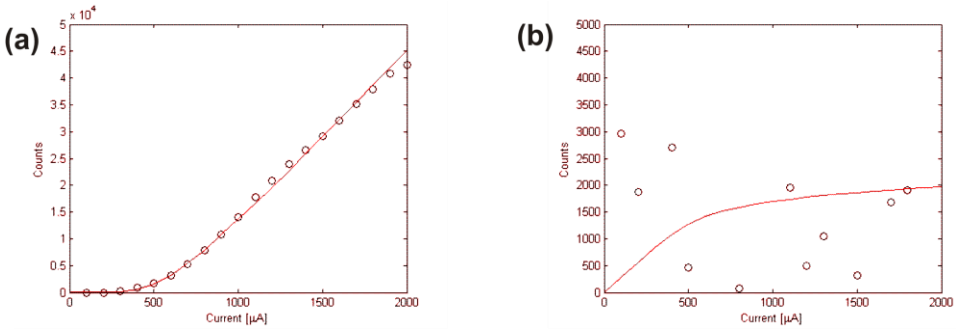

Fig. 6. (a) Light in the lasing mode versus injection current (circles). Shows super-linear behavior and can be fit to a rate equation model (red line). (b) Circles give the extracted spontaneous emission outside the grating modes. The levels are very low compared to the lasing light and were indiscernible from the spectrometer noise. Red line is from rate equation model and is shown for completeness.

Spontaneous emission of light outside the grating modes is given in Fig. 6b. This spontaneous emission outside the Lorentzian functions associated with the cavity modes was very low, and at a level similar to the detector noise. The low spontaneous emission levels made it difficult to detect a definitive trend in the values.

#146774 - $15.00 USD Received 28 Apr 2011; revised 12 Jun 2011; accepted 14 Jun 2011; published 21 Jul 2011

The lasing wavelengths of a number of DFB devices with different core widths and grating periods is given in Fig. 5b. It can be seen that the wavelengths follow a trend associated with the grating period. The bulk InGaAs gain material used in the devices has higher maximum gain due to increased density of states, at shorter wavelengths. For wider waveguide widths, there is sufficient gain in the InGaAs core to permit lasing at the band gap mode resonance, which is close to 1500 nm. However, as the band gap mode resonance tends to longer wavelengths where there is less gain, or as the width of the waveguide is made smaller, then lasing occurs on a band edge mode, at shorter wavelengths, Fig. 5b. Note that for the band gap mode in particular, the laser wavelength is strongly affected by the size of the quarter wavelength shift section. A change in length of 1 nm for the shift section will result in a change in wavelength of approximately 3 nm. In some applications it may be desirable to have to have multiple phase shift sections in the cavity, or employ narrower bandwidth, lower reflection gratings via reduced waveguide width modulation [14].

To provide a point of comparison with DFB lasers, Fabry-Pérot type resonant cavity lasers [12] were also manufactured on the same semiconductor wafer as the DFB devices. The spectra for an FP device, with similar length to the DFB devices (~100 μm) and also at 80K, are shown in Fig. 7. Significant differences compared to the DFB cavity can be seen. In particular there are several lasing modes, furthermore there is a significant spontaneous emission pedestal in the spectra.

Via a numerical approach [22] it can be shown that perfect metal MISIM grating waveguides with $W_c < \sim\lambda/2$, can suppress the spontaneous emission into TM modes in the stop band by more than a factor of 100 in two dimensions and a factor of 2 in the third. Emission into all transverse electric modes is strongly suppressed. Additionally, as seen in other experiments [1,6], emission into the lasing mode can be significantly enhanced (up to a factor of 50) for emitters at the modal maximum. This three dimensional suppression may be superior to that in dielectric photonic crystal structures, where significant solid angles of the crystal do not experience the Bragg stop bands [23,24].

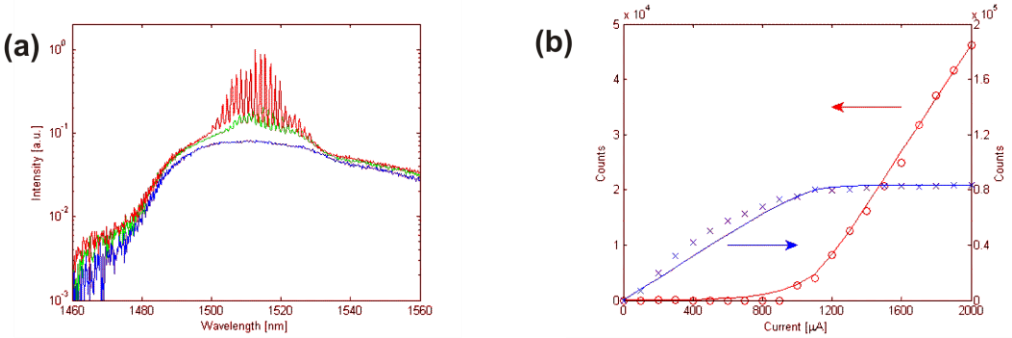

Fig. 7. (a) A number of spectra at various injection currents. Note the strong spontaneous emission pedestal. (b) Light in the lasing modes and also spontaneous emission outside the lasing modes. Note that when threshold is reached, spontaneous emission stays constant, indicating gain clamping. A rate equation model can reproduce the behavior with a realistic choice of parameters. Measurements were also at 80K.

For waveguides made of real metals the suppression in the stop bands is reduced, but is nevertheless significant with a typical suppression factor of 10. The spontaneous emission suppression manifests itself in the very low light levels in the DFB device at stop band wavelengths, and also in significantly lower threshold currents than the FP devices, Figs. 6b,7b. To quantify this behavior we have developed a rate equation model of the devices (see the next section for a detailed description). A reasonable agreement can be seen between the experiment and the simulation, Figs. 6,7.

A result of the broad band spontaneous emission suppression afforded by the metallic grating, is that the conditions for room temperature (RT, 296K) lasing are improved. Figure 8a shows the spectrum for an electrically pumped (pulsed operation) DFB device (with core

#146774 - $15.00 USD Received 28 Apr 2011; revised 12 Jun 2011; accepted 14 Jun 2011; published 21 Jul 2011

width ~140 nm +/– 10 nm). Figure 9a shows the light current curve. The light is strongly polarized in a direction consistent with a TM_0 mode. The results show strong linewidth reduction (Fig. 8b) and asuper-linear light current curve (Fig. 9a). Spontaneous emission outside the Lorentzian curves associated with the DFB cavity modes is low, unlike in the Fabry-Perot laser. This difficulty in precisely determining spontaneous emission prevents us from clearly showing gain clamping, which would definitely indicate lasing. The below threshold line width gives a cavity Q less than 100, less than expected from published optical loss values for silver [19]. We believe that the key issue here is the crystalline quality of the silver at the SiN_x interface, rather than surface roughness. More studies are required to optimize deposition and annealing techniques to obtain silver with optical losses as reported in [19].

Furthermore, the line width is broad (~9 nm), although comparable with other demonstrations of RT plasmon mode lasers [25]. The large linewidth may be due to cavity heating during the pulse. Or, strong spontaneous emission coupling to the mode, and that the true compensation of optical losses by the gain medium has not yet been achieved. In any case we expect refinements in the silver quality and other fabrication issues to improve future device performance.

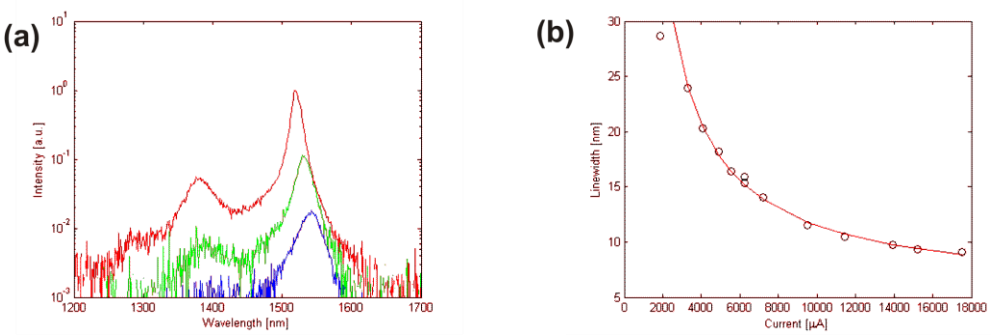

Fig. 8. (a) Spectra of a DFB cavity taken at a temperature of 296K at various injection currents, blue 2500μA, green 3600μA, red 7600μA. (b) Linewidth of the main peak as a function of injection current (circles). The red line is a fit to a $1/P_{mode}$ dependence.

This is the first demonstration of at least strong linewidth reduction and super-linear light-current curves for electrically pumped room temperature plasmon mode devices for the near infrared wavelengths. There have been several demonstrations of pulsed optically pumped plasmon mode devices [2,25]. However pulsed optical pumping generates little heating of the device. For electrical pumping, which can generate considerable device heating, it was not demonstrated yet if plasmon mode lasing was possible. Such RT lasing with a strongly confined plasmonic optical mode will be of critical importance for most applications.

#146774 - $15.00 USD Received 28 Apr 2011; revised 12 Jun 2011; accepted 14 Jun 2011; published 21 Jul 2011

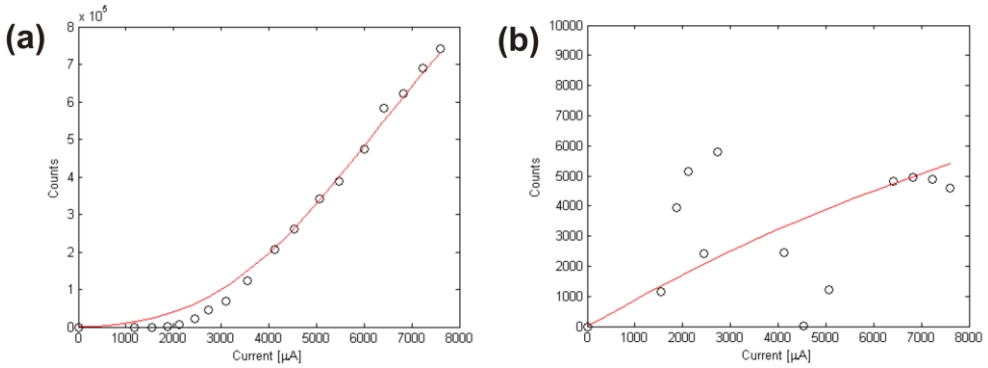

Fig. 9. (a) Plot of light versus current, extracted from the spectra, showing a super linear behavior and threshold around 2.5 milliamps. The red line is a rate equation model fit. (b) Circles show spontaneous emission levels as a function of injection current, showing a much lower level than the lasing mode light and also evidence of gain clamping at the higher injection levels. The red line is the rate equation model fit. Spontaneous emission counts were calculated by subtracting a Lorentzian fitted to the cavity modes from the total spectrum.

5. Rate equation model

To quantitatively interpret our measurements we developed a rate model for the carrier number N, and the photon number, S_i of the multiple optical modes that occur in the DFB and FP laser cavities:

$$\frac{dN}{dt} = \frac{I}{q} - \Gamma \upsilon_g g(n) \sum_i S_i - (A\frac{S_a}{V_a} + \gamma(n)Bn + Cn^2)N, \qquad (1)$$

$$\frac{dS_i}{dt} = (\Gamma \upsilon_g g(n) - \frac{1}{\tau_{p,i}})S_i + \gamma_i(n)BnN, \qquad i \in 1,2,...,m, \qquad (2)$$

where, I is the injection current, q the electronic charge, v_g the speed of light in the semiconductor, S_a the surface area of the active region exposed to SiN_x, V_a the active region volume, the carrier density $n = N/V_a$, $g(n)$ is the material gain, the photon lifetime $\tau_{p,i} = \lambda_i Q/(2\pi c)$, where c is the speed of light. Finally, A, B, C are the surface, bulk semiconductor radiative, and Auger recombination coefficients respectively [26]. The number of optical modes in the cavity m was taken as 75 for the FP cavity and two for the DFB cavity.

We employ a carrier density dependent emission enhancement factor $\gamma_i(n)$, which is calculated for each mode (3).

$$\gamma_i(n) = \int F_i \xi(n,\lambda) \frac{1}{1 + 4Q_i^2(\lambda/\lambda_i - 1)^2} d\lambda, \qquad i \in 1,2,...,m. \qquad (3)$$

Here the Purcell factor for the cavity is given by F_i. $\gamma_i(n)$ takes into account the spectral overlap of the normalized carrier energy distribution $\xi(n,\lambda)$, with each cavity resonance via the integral in (3). $\xi(n,\lambda)$ was determined by assuming a parabolic band model [26]. Emission into free space modes can still occur, due the finite length of the pillar under the InGaAs region. The factor F_{ext} accounts for this emission. Any spontaneous emission not going into free space modes is assumed to couple into the cavity modes i.e.

$$\gamma(n) = \sum_i \gamma_i(n) + F_{ext}. \qquad (4)$$

#146774 - $15.00 USD Received 28 Apr 2011; revised 12 Jun 2011; accepted 14 Jun 2011; published 21 Jul 2011

The model is fitted to the L-I measurement data obtained from the different devices. As a result we also obtain an expected trend for the spontaneous emission levels in the spectra, which are proportional to the carrier density.

The rate equation model used for the fabricated DFB lasers takes 2 modes into account, located at a wavelength of 1475 nm and 1405 nm. The first mode is the mode at the Bragg wavelength, the other mode is the band-edge mode. The corresponding Q-factors are 200 and 100 respectively; the corresponding Purcell coefficients are 5 and 1. The confinement factor was set to 0.20. The exposed surface and volume of the active region are $S_a = 7.2 \times 10^{-7}$ cm^2 and $V_a = 4.2 \times 10^{-12}$ cm^3.

For the Fabry-Pérot lasers, the number of modes is 75. The Q factor for all modes is 300 and the assumed Purcell factor is 0.01, which is equal to F_{ext}. The exposed surface and volume of the active region are $S_a = 6.0 \times 10^{-7}$ cm^2 and $V_a = 6.0 \times 10^{-12}$ cm^3. The confinement factor is 0.24. All simulations were carried out assuming an ambient temperature of 80K. A was 6.7 $\times 10^3$ cm/s and is related to the RT value [27] by a square root of absolute temperature relationship [28]. A was also varied slightly from published values to fit the initial slope of the integrated luminescence curve. B was taken as 9×10^{-10} cm^3/s, although there is some discrepancy between published values [26,29]. At low temperatures C does not play a significant role, but it was included for completeness and its value was 9.8×10^{-30} cm^6/s, one tenth of the RT value [26]. $g(n)$ was calculated assuming a parabolic band model [26].

Values of Q and F_{cav} used in the models were chosen to give a reasonable fit to the experimental data. However, for the DFB cavity these values were in the order of values expected from FDTD simulations, and given arguments about carrier distributions and diffusion in the cavities. For the Fabry-Pérot lasers the Purcell factors required to give a good fit were somewhat lower than simple calculations predict. The spontaneous emission coupling factor β is given by $\gamma_i(n)/\gamma(n)$ and is a function of n. The above threshold β are given along with the other model parameters below in Table 1.

Table 1. Rate Equation Model Parameters

DFB Laser (T = 80K)		*Fabry-Perot Laser (T = 80K)*	
β	**0.47**	**β**	**2×10^{-4}**
Q_1, Q_2	**200, 100**	**Q_{ave}**	**300**
F_1, F_2	**5, 1**	**F_{ave}**	**0.01**
λ	**1475 nm**	**λ_{center}**	**1510**
Γ	**0.20**	**Γ**	**0.24**
S_a	**7.2×10^{-7} cm^2**	**S_a**	**6.0×10^{-7} cm^2**
V_a	**4.2×10^{-12} cm^3**	**V_a**	**6.0×10^{-12} cm^3**
Modes	**2**	**Modes**	**75**

6. Conclusion

In summary we have shown that the DFB laser concept can be extended to plasmonic waveguides which confine light to below the diffraction limit. Bragg gratings are the premier method to control the wavelength of lasers and provide wavelength dependent mirrors with controllable reflectivity. Furthermore, Bragg gratings in active MIM waveguides can be designed for very wide bandwidth and a coupling coefficient much higher than in dielectric gratings, and can lead to strong spontaneous emission suppression. This spontaneous emission suppression can reduce the threshold current and help in achieving room temperature electrically pumped operation in a gap-plasmon mode laser.

Acknowledgments

This work was supported by the Netherlands Organization for Scientific Research (NWO) through the "NRC photonics" grant, and by the Dutch Government MEMPHIS Grant.